

Calvin University

Calvin Digital Commons

University Faculty Publications and Creative Works

University Faculty Scholarship

10-21-2008

Estimating kinetic and thermodynamic parameters from single molecule enzyme-inhibitor interactions


Laura Porter-Peden
Calvin University

Sarah G. Kamper
Calvin University

Mark Vander Wal
Calvin University

Ronald Blankespoor
Calvin University

Follow this and additional works at: https://digitalcommons.calvin.edu/calvin_facultypubs

 Part of the [Molecular Biology Commons](#)

Recommended Citation

Porter-Peden, Laura; Kamper, Sarah G.; Wal, Mark Vander; and Blankespoor, Ronald, "Estimating kinetic and thermodynamic parameters from single molecule enzyme-inhibitor interactions" (2008). *University Faculty Publications and Creative Works*. 429.
https://digitalcommons.calvin.edu/calvin_facultypubs/429

This Article is brought to you for free and open access by the University Faculty Scholarship at Calvin Digital Commons. It has been accepted for inclusion in University Faculty Publications and Creative Works by an authorized administrator of Calvin Digital Commons. For more information, please contact digitalcommons@calvin.edu.

Estimating Kinetic and Thermodynamic Parameters from Single Molecule Enzyme–Inhibitor Interactions

Laura Porter-Peden, Sarah G. Kamper, Mark Vander Wal, Ronald Blankespoor, and Kumar Sinniah*

Department of Chemistry & Biochemistry, Calvin College, Grand Rapids, Michigan 49546

Received January 11, 2008

We report the application of recently developed microscopic models to estimate the apparent kinetic and thermodynamic parameters in a single molecule force spectroscopy study of the carbonic anhydrase enzyme and a complementary sulfonamide inhibitor. The most probable rupture force for the enzyme–inhibitor interaction shows a nonlinear dependency on the log-loading rate. Estimates for the kinetic and thermodynamic parameters were obtained by fitting the nonlinear dependency to linear cubic potential and cusp potential models and compared to the standard Bell–Evans model. The reliability of the estimated parameters was verified by modeling the experimental rupture force distributions by the theoretically predicted distributions at rupture. We also report that linkers that are attached to the enzyme and inhibitor show appreciable effects on the apparent kinetic and thermodynamic parameters.

Introduction

Single molecule force spectroscopy is a technique that provides unique information about the biomolecular interaction landscape that is hitherto not possible to obtain from conventional spectroscopy methods.^{1,2} In this technique, biorecognition molecules of interest are pulled apart or stretched under an external loading force. The experimentally observed rupture force is typically dependent on the external mechanical load. The distribution of rupture forces at a constant loading rate enables the prediction of the most probable rupture force, which is a quantitative measure of the biospecific interaction at that loading rate. A force spectrum of the single molecule interaction is generated by mapping the most probable rupture force as a function of the loading rate. Fitting the force spectrum data to different theoretical models yields kinetic and thermodynamic information for the single molecule interaction. The most commonly used theoretical model, the Bell–Evans phenomenological model, is a simple and convenient model for calculating estimates of the barrier width and the dissociation rate (the rate of dissociation at zero force) and providing a direct comparison to ensemble measurements in solution.^{3–5} However, this model has recently come under scrutiny, as it is based on the assumption that the barrier width is fixed under an external mechanical load. Further, recently developed microscopic models have demonstrated the limitations of the Bell–Evans model, especially at high and low loading rates, likely resulting in unreliable kinetic parameters.² The analytical expressions generated from the microscopic models can be used to model the rupture force distributions, to fit the force spectrum data assuming a single energy barrier, and to provide estimates for the barrier width, the dissociation rate, and the activation energy barrier. Additionally, the use of two different microscopic models to estimate the kinetic data allows for comparison of the estimates and

provides upper and lower bounds for the kinetic parameters. Since single molecule force spectroscopy data is best treated by microscopic models, these models provide a good starting point for exploring the experimental conditions that are often imposed upon biological interactions.

Techniques commonly used to study the kinetics of biomolecular interactions, such as optical tweezers or atomic force microscopy (AFM), require the biomolecules of interest to be tethered to tips and surfaces or beads. Determining how the tethers affect the kinetic parameters is of considerable interest. Woodside et al. have shown the kinetic rates to change by orders of magnitude when varying the base composition in DNA hairpins,⁶ while a 10-fold increase in handle lengths in a RNA hairpin study showed only minimal changes to the kinetic rates in studies based on optical tweezers.⁷ In AFM-based force spectroscopy measurements, it is fairly common to include poly(ethylene glycol) (PEG) groups in tethers used on probes and surfaces. These groups function to minimize nonspecific interactions and provide flexibility to the tether, which is a necessary requirement, especially in protein–ligand based interactions. Using PEG tethers of varying lengths, Ray et al. have shown the kinetic rates to be different by an order of magnitude in the interactions between hydrophobic hexadecane molecules.⁸ They further demonstrated that the kinetic parameters are significantly affected when the data analysis does not take the polymeric tethers into account. In this article, we report the effect of the tethers used to attach the carbonic anhydrase enzyme to a surface and the sulfonamide inhibitor to an AFM cantilever on the kinetics and thermodynamics of the single molecule interaction between the enzyme and the inhibitor.

Recently, we demonstrated that an active enzyme, carbonic anhydrase (CA), can be controllably oriented on charged surfaces by electrostatic immobilization.^{9,10} The enzyme was found to

* Corresponding author. Phone: (616) 526-6058. Fax: (616) 526-6501. E-mail: ksinniah@calvin.edu.

(1) Barsegov, V.; Klimov, D. K.; Thirumalai, D. *Biophys. J.* **2006**, *90*, 3827–3841.

(2) (a) Dudko, O. K.; Mathe, J.; Szabo, A.; Meller, A.; Hummer, G. *Biophys. J.* **2007**, *92*, 4188–4195. (b) Dudko, O. K.; Hummer, G.; Szabo, A. *Phys. Rev. Lett.* **2006**, *96*, 108101.

(3) Bell, G. I. *Science* **1978**, *200*, 618–627.

(4) Evans, E. *Annu. Rev. Biophys. Biomol. Struct.* **2001**, *30*, 105–128.

(5) Evans, E. *Faraday Discuss.* **1999**, *111*, 1–16.

(6) Woodside, M. T.; Behnke-Parks, W. M.; Larizadeh, K.; Travers, K.; Herschlag, D.; Block, S. M. *Proc. Natl. Acad. Sci. U.S.A.* **2006**, *103*, 6190–6195.

(7) Wen, J.-D.; Manosas, M.; Li, P. T. X.; Smith, S. B.; Bustamante, C.; Tinoco, I.; Ritort, F. *Biophys. J.* **2007**, *92*, 2996–3009.

(8) Ray, C.; Brown, J. R.; Akhremitchev, B. B. *J. Phys. Chem. B* **2007**, *111*, 1963–1974.

(9) Wang, X.; Zhou, D.; Sinniah, K.; Clarke, C.; Birch, L.; Li, H.; Rayment, T.; Abell, C. *Langmuir* **2006**, *22*, 887–892.

(10) Kamper, S. G.; Porter-Peden, L.; Blankespoor, R.; Sinniah, K.; Zhou, D.; Abell, C.; Rayment, T. *Langmuir* **2007**, *23*, 12561–12565.

Chart 1. Molecular Structures of Inhibitor Molecules Used in This Study: Tether I, Tether II, and 29-Mercapto-3,6,9,12,15,18-hexaoxonacosan-1-ol (III)

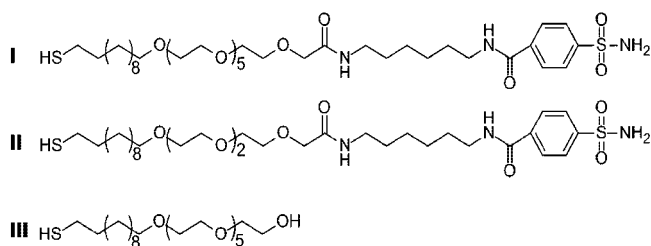
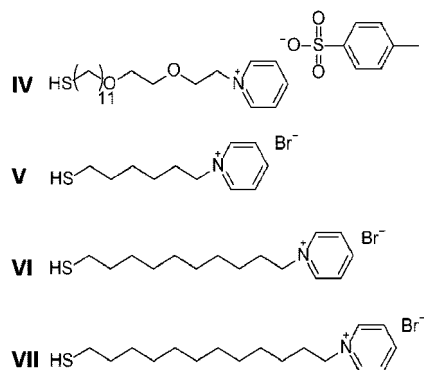


Chart 2. Molecular Structure of Enzyme Linker Molecules Used in This Study: *N*-[3,6-Dioxa-17-(mercaptoheptadecyl)pyridinium Tosylate (IV), *N*-(6-Mercaptohexyl)pyridinium Bromide (V), *N*-(10-Mercaptododecyl)pyridinium Bromide (VI), and *N*-(12-Mercaptododecyl)pyridinium Bromide (VII)



form a complete layer on both the positively (terminated with a pyridinium salt) and negatively (terminated with a carboxylic acid) charged surfaces, however, with different orientations. On the positively charged surface, the enzyme is oriented such that the active site is predominantly pointed upward, while on the negatively charged surface the enzyme is oriented such that the active site is predominantly pointed downward. We examined the immobilization of CA on pyridinium linkers of different lengths including one with an ethylene glycol group incorporated into the linker. The catalytically active site of CA was probed using a tethered *p*-carboxybenzenesulfonamide (CBS) inhibitor containing a hexa(ethylene glycol) spacer and compared to results from a recent study which examined this interaction with the CBS inhibitor containing a tri(ethylene glycol) spacer.¹⁰ For comparison, the inhibitors (**I** and **II**) are shown in Chart 1. The diluent molecule (**III**) ensures a very low density of inhibitor molecules is on the AFM probe, which is required for observing single molecule interactions. To optimize the observed rupture interactions between the CA enzyme and the sulfonamide inhibitor, thereby minimizing the time required for collecting force–distance data and the damage to the mechanical sensor, the positively charged pyridinium linker was varied in length (see Chart 2). Varying the inhibitor tether length and the enzyme linker length allowed us to examine the effect of these experimental variables on the kinetic and thermodynamic parameters of the single molecule enzyme–inhibitor interaction.

Experimental Section

Materials. Carbonic anhydrase II from bovine erythrocytes, tetrahydrofuran (THF, HPLC grade), 11-mercapto-1-undecanol (97%, MCU), and sodium acetate buffer (3 M, 0.2 μ m filtered) were purchased from Sigma-Aldrich (St. Louis, MO). Sodium acetate buffer was purchased at a 3 M concentration and adjusted to

experimental concentrations (20 mM NaOAc, 100 mM NaCl, pH 4.8) using NaCl (Mallinckrodt, Hazelwood, MO) and ultrapure water (18.2 M Ω -cm resistivity) obtained from a Barnstead water purifier (Fisher Scientific). This buffer was filtered (0.2 μ m pore size) prior to use in force spectroscopy measurements and preparation of solutions. Ethanol (absolute, 200 proof) was purchased from AAPER Alcohol and Chemical Co. (Shelbyville, KY) and filtered (0.2 μ m pore size) prior to use. The synthesis of **I**–**VII**, some of which are known in the literature,¹¹ are included in Supporting Information.

Substrate and Probe Preparation. Preparation of ultraflat template-stripped gold (TSG) surfaces was performed as previously reported.¹² After stripping the mica layer, the gold surfaces were washed using several milliliters of THF followed by several milliliters of ultrapure water. The gold surfaces were immediately placed into a 1.0 mM solution of enzyme linker in ethanol and allowed to incubate for 20 h prior to use. Standard Si₃N₄ cantilevers (MLCT, Veeco Probes) were modified by 10 nm of chromium evaporation as an adhesion layer followed by 30 nm of gold evaporation (at a rate of 1 $\text{\AA}/\text{s}$). The tips were then placed immediately into a 1.0 mM total thiol solution and incubated for 20 h prior to use. To quantify the number of rupture events observed between the CA enzyme and the tethered inhibitor based on the varying lengths of the pyridinium linker, the surfaces and the tips were prepared by incubating the gold surfaces in a solution of one of the following: **IV**, **V**, **VI**, or **VII**, and by placing the tips in a solution of 1.0 mM **II** and 1.0 mM MCU (both in ethanol) in a 1:20 ratio. For loading rate dependence studies, the gold surfaces were incubated in a solution of either **IV** or **VII** and the tips were incubated in a solution of 1.0 mM **I** and 1.0 mM **III** (both in ethanol) in a 1:50 ratio. To examine the effect of the inhibitor to diluent ratio, a gold surface was incubated in a solution of **IV**, while tips were incubated in a solution of 1.0 mM **I** and 1.0 mM **III** (both in ethanol) combined in one of the following ratios: 1:20, 1:50, or 1:100. Before each force spectroscopy experiment, a surface was removed from the pyridinium linker solution, rinsed with NaOAc buffer and ultrapure water, and placed in a 0.1 mg/mL solution of CA in NaOAc buffer for 1 h.

Instrumentation. All force spectroscopy experiments were performed using a PicoForce atomic force microscope (Veeco Metrology, Santa Barbara, CA) equipped with a 40 μ m scanner (20 μ m in the *z* direction). Spring constants of gold-coated Si₃N₄ cantilevers were measured using the thermal fluctuation method.¹³ To access a wide range of loading rates, several different cantilevers were used, with nominal spring constants of 42–134 pN/nm. The nominal spring constants of each cantilever used across multiple days were within the typical tolerance of 20%.

AFM Imaging of Enzyme Surface. For scratching the enzyme and linker layer, a small scan area was selected at a specific region, and the set point voltage was increased by several units until the surface structure of the TSG was observed. After the enzyme and linker layer were scratched, the AFM tip was fully retracted from the surface by decreasing the set point voltage, zoomed out to a bigger scan area, then re-engaged with the minimum force required to record the topographic images. This procedure was performed for enzymes immobilized on linkers **V**, **VI**, and **VII**.

Force Spectroscopy Measurements. Force spectroscopy measurements and data analysis were performed similarly to previously described methods.¹⁰ Briefly, force measurements were conducted in a glass fluid cell (Veeco Instruments) at room temperature (23–24 $^{\circ}\text{C}$) in sodium acetate buffer (20 mM NaOAc, 100 mM NaCl, pH 4.8). The ramp size was set to 250 nm, the surface delay to 1 s, and the loading (contact) force to 100 pN. Loading rate dependence studies were carried out with apparent loading rates from 660–70 000 pN/s. The apparent loading rate was obtained by taking the product

(11) (a) Zhou, D.; Wang, X.; Birch, L.; Rayment, T.; Abell, C. *Langmuir* **2003**, *19*, 10557–10562. (b) Prime, K. L.; Whitesides, G. M. *J. Am. Chem. Soc.* **1993**, *115*, 10714–10721. (c) Yokokawa, S.; Tamada, K.; Ito, E.; Hara, M. *J. Phys. Chem. B* **2003**, *107*, 3544–3551. (d) Pale-Grosdemange, C.; Simon, E.; Prime, K.; Whitesides, G. *J. Am. Chem. Soc.* **1991**, *113*, 12–20.

(12) Vander Wal, M.; Kamper, S.; Headley, J.; Sinniah, K. *Langmuir* **2006**, *22*, 882–886.

(13) Hutter, J. L.; Bechhoefer, J. *Rev. Sci. Instrum.* **1993**, *64*, 1868–1873.

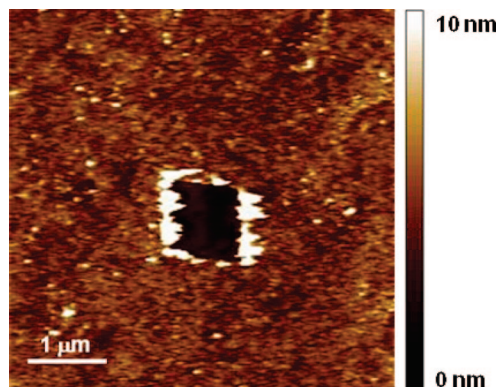


Figure 1. Topography of the electrostatically immobilized CA enzyme on the pyridinium linker **VII**. A $1\ \mu\text{m}^2$ scratched region in the center of the image was used to determine the thickness of the enzyme layer ($\sim 4\ \text{nm}$). White protrusions around the scratched area are most likely the result of stacked enzymes which were pushed away from the scratched region.

of the slope just prior to the rupture point and the pulling speed.^{8,14} Force measurements were performed for $\sim 1\ \text{h}$, in at least 5–10 random spots on the surface, until approximately 60–70 specific rupture force curves were collected from a total of approximately 100–500 force–distance curves at a specific loading rate. Only force curves that indicated an extension of the force curve followed by an abrupt rupture of the retraction force curve were binned for data analysis.

All force–distance curves were analyzed using the DI Nanoscope offline software provided by Veeco Metrology (version 6.13R1). Force data was analyzed using the freeware statistical package R (<http://www.r-project.org/>). Kernel density function plots were generated to examine the distribution of forces. All density curves reported were generated using 512 points and the Gaussian kernel function. The most probable rupture force was obtained by fitting the density curve to one (or more for multiple events) Gaussian and taking the peak value of the Gaussian representing the single molecule rupture event. The error of the most probable rupture force is reported to two standard deviations. The theoretical models that were fit to loading rate dependence data generated kinetic and thermodynamic parameters, and the uncertainties associated with these parameters are reported as standard error reported by the SigmaPlot program used for the fitting analysis.

Results and Discussion

Topography of Immobilized Enzyme Surface. The electrostatically immobilized CA enzyme surface was imaged by AFM where the enzyme was electrostatically attached to the linkers **V**, **VI**, or **VII**. A representative image of the CA immobilized surface shows the morphology of the CA enzyme surface which appears to be both smooth and homogeneous (Figure 1). A $1\ \mu\text{m}^2$ region of the surface was removed by applying higher forces to determine the thickness of the CA enzyme layer. The experimentally determined thickness of $\sim 4\ \text{nm}$ by AFM compares favorably with the dimensions of the CA enzyme ($3.9 \times 4.2 \times 5.5\ \text{nm}$),¹⁵ suggesting complete monolayer coverage of the CA enzyme on the surface containing the pyridinium linker **VII**. However, when the CA enzyme was immobilized on either **V** or **VI** and a $1\ \mu\text{m}^2$ region was removed by applying a higher force, the topography of the surface failed to show the indented region. This is most likely due to the indented region being refilled by the more fluid-like **V** or **VI** molecules, whereas the

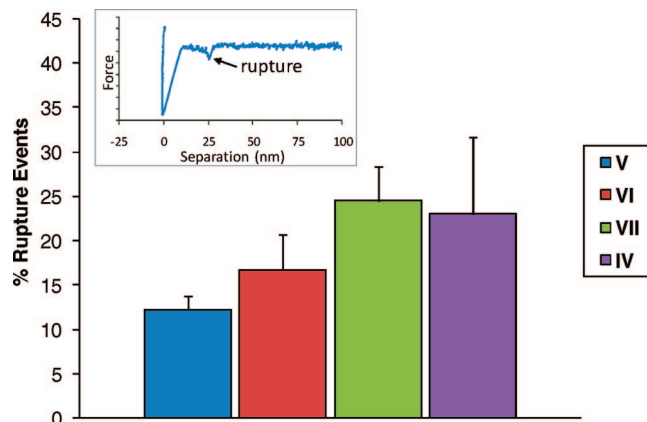


Figure 2. Percentage of rupture events from all force curves observed between the inhibitor **II** and CA enzyme on SAMs of four different enzyme linker molecules. Error bars represent standard deviation. The AFM tip was functionalized with **II** diluted with MCU in a 1:20 ratio. The inset highlights a force distance curve representing an adhesion event followed by an extension and a rupture event.

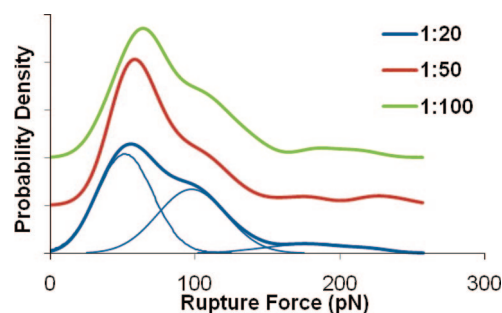


Figure 3. Force distributions demonstrating the most probable rupture force for the enzyme–inhibitor interaction using probes with the inhibitor (**I**) to diluent (**III**) ratios of 1:20, 1:50, and 1:100. The TSG surface was prepared with a SAM of **IV** prior to electrostatic immobilization of CA enzyme. Each force distribution represents 60–70 rupture events. Gaussians were used to fit force distributions to identify the most probable single molecule rupture force and the simultaneous multiple rupture events (indicated on 1:20 dilution rupture force distribution).

linker molecule **VII**, with a 12-carbon chain, is more likely to be crystalline and to form a stable and homogeneous self-assembled monolayer.

Effect of Enzyme Linker Length on Percentage of Rupture Events. Previous work has demonstrated that CA enzyme immobilized on a positively charged pyridinium surface increases the number of specific interactions between the catalytically active site of the enzyme and a tethered sulfonamide inhibitor in comparison to covalent immobilization methods which result in random orientation of the enzyme.⁹ We have examined CA immobilized on pyridinium linkers of increasing carbon chain lengths (**V**, **VI**, **VII**) and a pyridinium linker that contains a diethylene glycol group (**IV**) to minimize nonspecific interactions between the enzyme and linker. Rupture events observed between the CA enzyme and the sulfonamide inhibitor (**II**) are indicative of a specific interaction (see inset in Figure 2). The percentage of rupture events observed between the enzyme and the tethered inhibitor increased with increasing length of the linker molecule on which the CA enzyme was attached. The shorter pyridinium linkers (**V** and **VI**) resulted in approximately 10–15% rupture events, while **VII** and **IV** resulted in approximately 25% rupture events. This result further confirms the stability of the enzyme monolayer on linkers **IV** and **VII**. However, it is possible that the enzyme is not as uniformly distributed or that enzyme motion during contact between the inhibitor and the enzyme hinders

(14) Meadows, P. Y.; Bemis, J. E.; Walker, G. C. *J. Am. Chem. Soc.* **2005**, *127*, 4136–4137.

(15) Håkansson, K.; Carlsson, M.; Svensson, L. A.; Liljas, A. *J. Mol. Biol.* **1992**, *227*, 1192–1204.

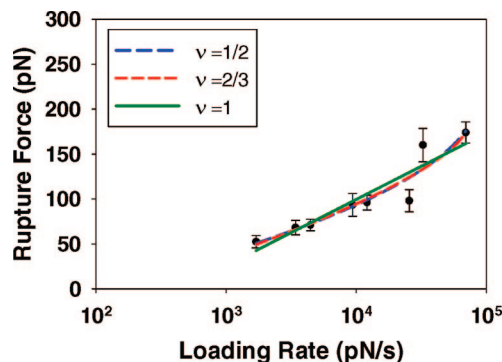


Figure 4. Dynamic force spectrum for the I–VII system. The rupture force is the peak rupture force obtained from a density function plot highlighting the most probable rupture event arising from a single molecule interaction. The rupture force versus apparent loading rate data were modeled by cusp potential model ($\nu = 1/2$), linear cubic potential model ($\nu = 2/3$), and the Bell–Evans model ($\nu = 1$). The kinetic and thermodynamic parameters obtained from the fits are given in Table 1.

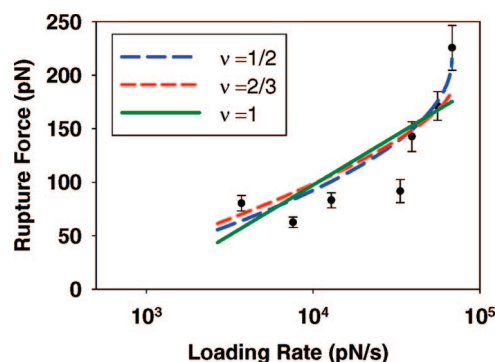


Figure 5. Dynamic force spectrum for the I–IV system. The rupture force versus apparent loading rate data were modeled by cusp potential model ($\nu = 1/2$), linear cubic potential model ($\nu = 2/3$), and the Bell–Evans model ($\nu = 1$). The kinetic and thermodynamic parameters obtained from the fits are given in Table 1.

Table 1. Kinetic and Thermodynamic Parameters for Systems Utilizing Different Enzyme Linker Molecules

	ν	ΔG^\ddagger (kcal/mol)	x^\ddagger (nm)	k_0 (s ^{−1})
I–VII	1/2	4.0 ± 0.7	0.25 ± 0.11	6.6 ± 7.9
	2/3	3.6 ± 0.6	0.21 ± 0.07	8.4 ± 7.3
	1	-	0.13 ± 0.02	14.0 ± 6.3
I–IV	1/2	3.5 ± 0.4	0.22 ± 0.02	10.3 ± 3.3
	2/3	3.5 ± 0.8	0.19 ± 0.05	9.0 ± 8.2
	1	-	0.10 ± 0.02	22.5 ± 10.3

specific interactions for enzymes immobilized on linkers **V** and **VI**. Nevertheless, the percent rupture events observed is significantly greater than the 1–2% of rupture events observed when the CA enzyme was covalently attached via amine coupling methods.¹⁶ The data in Figure 2 also demonstrates that both linker **IV** and **VII** are suitable for examining the enzyme–inhibitor interaction at varying loading rates since the high percent observation of rupture events would reduce the amount of time spent collecting data and thereby minimize damage to the probe and limit contamination of the enzyme immobilized surface.

Single Molecule Interactions by Inhibitor Dilution. To observe single molecule interactions in protein–ligand-based force spectroscopy experiments, the biorecognition molecules on the tip or surface need to be diluted by an appropriate molecule

Table 2. Modified Apparent Kinetic and Thermodynamic Parameters for the Carbonic Anhydrase Enzyme and Sulfonamide Inhibitor Systems II–VII, I–VII, and I–IV

	ν	ΔG^\ddagger (kcal/mol)	x^\ddagger (nm)	k_0 (s ^{−1})
II–VII ^a	1/2	5.4 ± 1.7	0.51 ± 0.35	0.81 ± 3.2
	2/3	4.8 ± 2.0	0.42 ± 0.34	1.2 ± 3.7
	1	-	0.29 ± 0.05	3.4 ± 2.8
I–VII	1/2	4.4 ± 0.8	0.23 ± 0.10	6.6 ± 7.9
	2/3	3.9 ± 0.6	0.19 ± 0.06	8.4 ± 7.3
	1	-	0.13 ± 0.02	14.0 ± 6.3
I–IV ^b	1/2	3.5 ± 0.4	0.22 ± 0.02	10.3 ± 3.3
	2/3	3.5 ± 0.8	0.19 ± 0.05	9.0 ± 8.2
	1	-	0.10 ± 0.02	22.5 ± 10.3

^a The apparent kinetic and thermodynamic parameters for the enzyme–inhibitor system, II–VII were reported previously,¹⁰ while in this data ΔG^\ddagger and x^\ddagger were adjusted by 20% to get reasonable theoretical fits to the force distributions (see Supporting Information). ^b The force distributions were fitted well for a range of loading rates without changes to ΔG^\ddagger and x^\ddagger obtained from eq 1.

which is not involved in the primary interaction of interest. Although higher dilutions of the inhibitor molecule on the probe will invariably result in single molecule rupture events, the time required to collect an adequate number of rupture events based on specific interactions will be significantly greater. When diluting the inhibitor molecules on the probe, a tradeoff is often required between only observing single molecule interactions and observing a high percentage of single molecule interactions with some multiple interactions. Inhibitor molecules on the AFM probe were diluted in the ratios of 1:20, 1:50, and 1:100 (I:III). Figure 3 displays the force distributions obtained from the interactions between CA enzyme and the tethered inhibitor for three functionalized probes containing different inhibitor:diluent ratios. Each of the force distribution plots show a rupture occurring from a single enzyme–inhibitor interaction as well as the simultaneous rupture occurring from multiple enzyme–inhibitor interactions, as seen from the accompanying high-force tail.¹⁷ The dilution of the inhibitor molecules on the probe by a factor of 100 does not appear to remove the high force tail, indicating that simultaneous multiple bond rupture events are very likely in protein–ligand type interaction studies by single molecule force spectroscopy. The force rupture distribution data can be fitted with Gaussians to determine the most probable rupture force for the single molecule interaction, as shown for the 1:20 dilution data in Figure 3. For the 1:20 dilution case, the two major peaks that appear in the distribution are separated by approximately 50 pNs. This enables us to assign the peak at ~50 pN to the single molecule rupture events and the peak at ~100 pN to the simultaneous rupture of two enzyme–inhibitor interaction events. Both peaks are clearly discernible in the force distribution data for each of the three dilutions. The magnitude of the most probable rupture force for the single molecule interaction (between 50–60 pN) appears to be within experimental error for the three inhibitor probes of different dilutions.

Estimating Apparent Kinetic and Thermodynamic Parameters. Applying an external force to rupture protein–ligand interactions in single molecule force spectroscopy provides a unique and powerful method to obtain kinetic and thermodynamic information about biomolecular interactions. Determining how the tethers and linkers attached to the biosensing molecules factor into the kinetic or thermodynamic parameters has been of considerable interest. Although previous studies have examined the enzyme–inhibitor interaction, the presence of the tether was only taken into account for computing the apparent loading rate.¹⁰ In this study, we compared the loading rate dependence of the

(16) Wang, X. Z. Ph.D. Thesis, University of Cambridge, Cambridge, U.K., 2003.

(17) Sulchek, T.; Friddle, R. W.; Noy, A. *Biophys. J.* **2006**, *90*, 4686–4691.

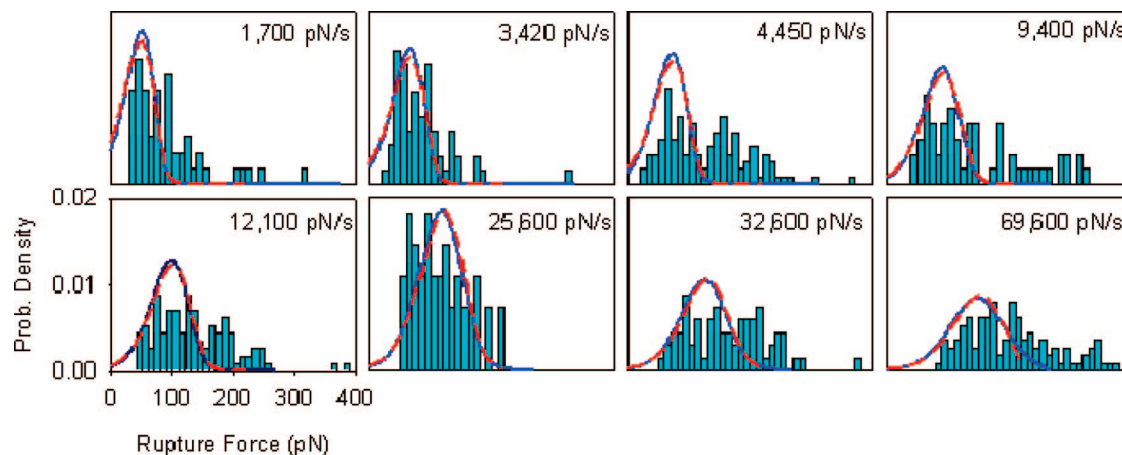


Figure 6. Distribution of forces at rupture from eq 2 overlaid on experimental distributions for the **I–VII** system. Histograms represent the normalized experimental distribution of all observed enzyme–inhibitor interactions. Predicted distributions plotted from eq 2 used values for ΔG^\ddagger and x^\ddagger adjusted by $\sim 10\%$ from the values obtained from eq 1. The blue trace indicates the fit for the scaling parameter, $\nu = 1/2$, and the red trace indicates the fit for $\nu = 2/3$.

CA enzyme–sulfonamide inhibitor interaction while changing the length of the tethered inhibitor and/or the length of the linker molecules to which the enzyme was electrostatically attached. Varying the length of either the inhibitor tether and/or the enzyme linker enabled us to predict how these experimental variables may affect the apparent kinetics and thermodynamics of the interaction. Two systems of inhibitor tether and enzyme linker were studied: **I** with **IV** and **I** with **VII**. Both were compared to a previously reported system of **II** with **VII**.¹⁰ For each enzyme–inhibitor system, the rupture force was measured at various loading rates. The most probable rupture force at each loading rate was obtained by fitting the force distribution data to a Gaussian as previously reported.¹⁰ The apparent loading rates used in the **I–IV** system were 2600–68 300 pN/s, while the apparent loading rates used in the **I–VII** system were 1700–69 600 pN/s. Figures 4 and 5 show the most probable rupture force versus the apparent loading rate for **I–IV** and **I–VII** enzyme–inhibitor systems. The loading rate dependence data for each system was fitted to the theoretical models proposed by Dudko et al.² where the most probable rupture force, F , is plotted as a function of the loading rate, r , according to eq 1,

$$F \cong \frac{\Delta G^\ddagger}{\nu x^\ddagger} \left\{ 1 - \left[\frac{1}{\beta \Delta G^\ddagger} \ln \frac{k_0 e^{\beta \Delta G^\ddagger}}{\beta x^\ddagger r} \right]^\nu \right\} \quad (1)$$

where ΔG^\ddagger is the activation free energy, ν is a scaling factor inherent for each model, x^\ddagger is the barrier width, k_0 is the dissociation rate constant, and β is $(k_B T)^{-1}$, where k_B is the Boltzmann constant and T is absolute temperature. Both Figures 4 and 5 show that the most probable rupture force is a nonlinear function of the log-loading rate. The apparent kinetic and thermodynamic parameters were obtained from the two microscopic models: the cusp potential model ($\nu = 1/2$) and the linear cubic potential model ($\nu = 2/3$) and compared to the Bell–Evans model ($\nu = 1$). The estimated parameters represent the entire system and therefore include contributions from both the enzyme–inhibitor complex and the linker molecules. Estimates for the kinetic and thermodynamic parameters for the **I–IV** and **I–VII** enzyme–inhibitor systems are given in Table 1. The two different microscopic models give parameter values that are similar, while the Bell–Evans model appears to consistently underestimate the barrier width and overestimate the dissociation rate constant. As can be seen from ΔG^\ddagger , x^\ddagger , and k_0 values in Table 1, the different enzyme linkers used for the **I–IV** and

I–VII systems have little to no effect on the thermodynamic parameters. This result is not surprising since the enzyme linker is not involved in the primary interaction between the sulfonamide inhibitor and the active site of the carbonic anhydrase enzyme. However, comparison of the **I–VII** system with the previously reported enzyme–inhibitor system (**II–VII**) shows significant differences in the apparent kinetic and thermodynamic parameters. The activation free energy was determined to be ~ 5 kcal/mol for the **II–VII** system (Table 2),¹⁰ while ~ 1 kcal/mol reduction in the activation barrier is observed when using the longer inhibitor tether (**I**). The major difference between the **I–VII** and the **II–VII** systems is the additional PEG groups in the inhibitor tether. Therefore, it appears that the incorporation of three additional PEG groups into the inhibitor tether, which effectively increases the length of the tether, has a significant effect on the kinetics of the single molecule enzyme–inhibitor interaction by increasing k_0 by nearly 1 order of magnitude in comparison to the **II–VII** system, where k_0 is ~ 1 s^{−1}. A similar increase in k_0 while increasing the linker length was reported by Ray et al.,⁸ when examining the rupture forces between hexadecane molecules that were tethered by short and long PEG linkers. Such an increase in k_0 with increase in tether length is not unexpected based on theory, because the effect of the linker is to soften the overall effective spring constant. The large uncertainties accompanying k_0 values are most likely due to the scatter in the force spectrum data and are similar in magnitude to what has been reported in the literature.^{8,17} In bulk solution studies, the dissociation rate constant for the free CBS in solution and CA **II** enzyme by surface plasmon resonance (SPR) was reported to be 0.037 s^{−1}.¹⁸ On the basis of this result, the height of the energy barrier for the naturally spontaneous dissociation was calculated to be 19.4 kcal/mol.¹⁰ Clearly, the energy barrier is lowered significantly under the influence of an external force irrespective of the length of the linkers used. The faster escape rates shown in Table 1 are most likely a result of the lowering of this energy barrier. However, we caution that the bulk conditions used in the SPR study and the single molecule conditions used in our studies are different. Specifically, the single molecule studies were performed at a pH of 4.8 (one unit below the pI of the enzyme) in order to ensure the attachment of the enzyme to the surface, while the SPR study

(18) Day, Y. S. N.; Baird, C. L.; Rich, R. L.; Myszkowski, D. G. *Protein Sci.* **2002**, *11*, 1017–1025.

was performed at a pH of 7, a pH at which the enzyme does not attach to the surface.

The apparent kinetic and thermodynamic parameters obtained using the microscopic models can be further validated and improved by the analysis of the distribution of the rupture forces obtained from the enzyme–inhibitor interactions at different loading rates. On the basis of the microscopic models,² the distribution of forces at rupture is given by eq 2

$$p(F|\nu) = (r)^{-1} k(F) \exp \left[\frac{k_0}{\beta x^\ddagger r} \right] \exp \left[\frac{-k(F)}{\beta x^\ddagger r} \left(1 - \frac{\nu F x^\ddagger}{\Delta G^\ddagger} \right)^{1-(1/\nu)} \right] \quad (2)$$

and, $k(F)$, the force-dependent rate is given by eq 3.

$$k(F) = k_0 \left(1 - \frac{\nu F x^\ddagger}{\Delta G^\ddagger} \right)^{(1/\nu)-1} \exp \left\{ \beta \Delta G^\ddagger \left[1 - \left(1 - \frac{\nu F x^\ddagger}{\Delta G^\ddagger} \right)^{1/\nu} \right] \right\} \quad (3)$$

The estimates obtained for k_0 , ΔG^\ddagger , and x^\ddagger from eq 1 for the enzyme–inhibitor systems were incorporated into eq 2, and the distribution of forces at rupture, $p(F|\nu)$, was plotted for each loading rate and overlaid on the normalized experimental distributions. For the **I–VII** enzyme–inhibitor system, shown in Figure 6, the experimental rupture force distributions are from both single and multiple enzyme–inhibitor bond rupture events, while the theoretical rupture force distributions were obtained using eq 2 after adjusting ΔG^\ddagger and x^\ddagger by $\sim 10\%$ from the values obtained from eq 1. The theoretical distributions appear to fit the single molecule enzyme–inhibitor interactions reasonably well at all loading rates, given that the microscopic models do not incorporate multiple bond rupture events. Furthermore, the theoretical fits appear to show no difference for $\nu = 1/2$ and $\nu = 2/3$, suggesting that the fit is insensitive to the precise shape of the free energy profile and is most likely model independent. The theoretical distribution of forces also appear to be fairly sensitive to changes in ΔG^\ddagger and x^\ddagger while insensitive to changes in k_0 . The modified kinetic and thermodynamic parameters for the **I–VII** interactions are shown in Table 2. Force distributions obtained from the **I–IV** and **II–VII** enzyme–inhibitor systems were also fitted using equation 2 and the figures are shown in

the Supporting Information (Figures S3 and S4). The modified apparent kinetic and thermodynamic parameters for **I–IV** and **II–VII** are shown in Table 2 for comparison of the different handles used for attaching the carbonic anhydrase enzyme and the sulfonamide inhibitor to an AFM surface and tip, respectively. The results shown in Table 2 suggest that the perturbation induced by the inhibitor tether appears to have an effect on the apparent kinetics and thermodynamics of the enzyme–inhibitor system, while the handles used for attaching the carbonic anhydrase enzyme to the surface play a minimal role.

Conclusions

The extent to which the linkers and tethers attached to enzymes and inhibitors factor into the kinetic and thermodynamic parameters was investigated by studying the single molecule interactions between CA enzyme and a tethered sulfonamide inhibitor. The CA enzyme immobilized on longer carbon chain linker molecules show a higher percentage of specific interactions. Apparent kinetic and thermodynamic parameters estimated from loading rate dependence studies were used in determining the theoretical rupture force distributions at various loading rates for the carbonic anhydrase–sulfonamide inhibitor system. The rupture force distributions based on the two microscopic models with $\nu = 1/2$ and $\nu = 2/3$ showed no difference. The enzyme linker appears to have minimal effect on the apparent kinetic and thermodynamic parameters, while an increase in length of the inhibitor tether demonstrates a significant effect on the kinetics.

Acknowledgment. This work was supported by the National Institutes of Health (grant 1R15GM073662-01). We thank Dr. Olga Dudko (UCSD) and Dr. Boris Ahkremitchev (Duke) for helpful discussions and suggestions. Stephanie Hoogendoorn and Phil Homan are thanked for the synthesis of some of the organic molecules used in this study. R.B. acknowledges the support of the Brummel Chair at Calvin College.

Supporting Information Available: Synthesis of the molecules and force distribution data analysis. This material is available free of charge via the Internet at <http://pubs.acs.org>.

LA801477A